Energy Conversion and Management 287 (2023) 117107

Contents lists available at ScienceDirect

Energy Conversion and Management

journal homepage: www.elsevier.com/locate/enconman

Investigation of the effect of hidden vortex generator-flap integrated mechanism revealed in low velocities on wind turbine blade flow

Mustafa Özden [a,b], Mustafa Serdar Genç [a,c,*], Kemal Koca [d]

[a] Wind Engineering and Aerodynamic Research Laboratory, Department of Energy Systems Engineering, Erciyes University, 38039 Kayseri, Turkey
[b] Scientific Research Projects Unit of Erciyes University, Erciyes University, 38039 Kayseri, Turkey
[c] Energy Conversion Research and Application Center, Erciyes University, 38039 Kayseri, Turkey
[d] Department of Mechanical Engineering, Abdullah Gül University, 38080 Kayseri, Turkey

ARTICLE INFO

Keywords:
Airfoil
Vortex generator-flap integrated mechanism
Flow control
Wind turbine

ABSTRACT

In this study, the flap and vortex generator (VG) mechanisms which were employed separately in aircraft were used as integrated first in literature. In this mechanism, the flap motion triggered and activated the VGs when it was needed at low speeds. Thus, this flap mechanism eliminated the unnecessary drag force generation when VGs were not needed. Numerical simulations which were validated with experimental data were employed in the study. In the first step, the flow characteristics formed on the S809 airfoil with 4 different flap angles ($\beta = 30°$, 20°, 10°, 0°) were investigated without the VG. Then, those flow structures formed on the S809 airfoil with both flap and VG were examined under the same conditions. According to the results, utilizing flap and VGs together had a positive impact at low wind speeds. Moreover, due to the flap and vortex generator integrated mechanism closed up to be not unnecessary drag formation at high wind speeds, thus those structures increased further to the positive effect with the increasing wind velocity. In terms of energy output, it was shown that this novel idea provided more energy output in this study.

1. Introduction

A wind turbine can be operated in a wide range of angles of attack in the field. The variation of angles of attack or other external conditions can cause the flow separation or stall to form over wind turbine blades [1-4]. Flow separation and stall phenomena are undesirable conditions for wind turbine blades and can reduce their aerodynamic performance, causing high fatigue-external loads, lower energy outputs and aerodynamic noises [3-5]. Therefore, they need to avoid flow separation and stall. In this respect, the flow near the wall and in the boundary layer must have adequate momentum. This assists the boundary layer to resist the effects of adverse pressure gradients (APGs), which are responsible for flow separation. So far, different flow control methods have been performed to prevent flow separation and stall phenomena [6-8]. Although the active flow control methods have been still preferred, they have lagged behind the passive flow control techniques since they do not need external energy [9-12]. Those passive flow control techniques can be assorted as follows: employing roughness material [13] and riblet [14], enforcing slots [15], taking into account the dimples [16] and grooves [17], utilizing flexibility [18-24], performing bio-inspired applications [25-30], installing vortex generators (VGs) [31-33], and to name but a few. Besides these flow control studies, other studies were carried out to improve turbine performance by using different methods such as deflectors, concentrators or combined systems on wind turbines [34-38]. The results showed that these systems enhanced the maximum power coefficient of the turbine.

VGs have a broad reputation in the field since they are cost-effective and simple. They are essentially some pairs of vanes, and they protrude from the solid surface with or without having specific angles upstream of flow separation. It can be said that the vortices formed from the tips of

Abbreviations: Re, Reynolds number; LSB, Laminar Separation Bubble; VGs, Vortex Generators; APGs, Adverse Pressure Gradients; 3D, Three Dimensional; NREL, National Renewable Energy Laboratory; RANS, Reynolds-averaged Navier Stokes; AoA, Angle of Attack; max, Maximum; c, Chord Length; s, Span Length; F_L, Lift Force; F_D, Drag Force; C_L, Lift Coefficient; C_D, Drag Coefficient; α, Angle of Attack; β, Flap angle; ρ, Air Density; u, velocity; U_∞, Freestream Velocity; ω, Inverse Turbulent Time Scale; k_T, Turbulent Kinetic Energy; k_L, Laminar Kinetic Energy; y^+, A Ratio Between Turbulent and Laminar Influences in a Cell.

* Corresponding author at: Wind Engineering and Aerodynamic Research Laboratory, Department of Energy Systems Engineering, Erciyes University, 38039 Kayseri, Turkey.
E-mail address: musgenc@erciyes.edu.tr (M.S. Genç).

https://doi.org/10.1016/j.enconman.2023.117107
Received 27 February 2023; Received in revised form 12 April 2023; Accepted 23 April 2023
Available online 4 May 2023

VGs enhance the kinetic energy of the boundary layer by ensuring extra momentum and, hereby, flow separation or stall phenomena can be delayed, resulting in higher aerodynamic performance [39-43]. Pioneered study on VGs was performed by Taylor to postpone the boundary layer separation of aircraft wings [41]. Thenceforth, both experimental studies and numerical simulations have been carried out to learn how VGs have affected the flow field around wind turbine blades. It can be pointed out that there are two categories in terms of their investigation field, (i) one category examines the flow structures around airfoils in conjunction with VGs, (ii) the other category focuses on the optimization and design of VGs. The first choice primarily focuses on the results of installing VGs and how they work. For example, Nickerson [42] examined the aerodynamic properties of the NACA 0024 airfoil by using VGs at a low Reynolds number. His results pointed out that VGs were favorable when it was utilized at a 5% chord position. It was also indicated that the essential function of VGs was to decrease the effects of drag forces as the stall was controlled. The roles of VGs on thick airfoils were studied by Timmer and van Rooij [43]. They found that utilizing the VGs could postpone the stall angle with the increasing of the lift-drag ratio. A numerical simulation was performed to investigate the aerodynamic performance of the S809 airfoil with and without the VGs [44]. The results clearly showed that the thickness of the boundary layer was reduced by VGs, resulting in the presence of less viscous forces although the drag increased. Zhu et al. [45] studied numerically the control of the dynamic stall of the NREL S809 airfoil with both VGs and leading-edge roughness. The leading-edge roughness increased the turbulence kinetic energy and caused the separated flow and dynamic stall to occur early. The VGs raised near-wall kinetic energy and suppressed the separated flow.

The second option mainly tends to optimize the shapes and layouts of the VGs. In this regard, according to the review study performed by Lin [46] and Zhao et al [33], the site of the VGs installation should be close to the flow separation points. A study on NACA 4415 airfoil with the triangular and the rectangular VGs at Reynolds number 2×10^5 was studied by Fouatih et al. [47]. Their results clearly showed that the rectangular VGs produced more drag than the triangular VGs. An experimental study was performed to evaluate the performance of DU97-W-300 airfoil with VGs design [48]. Their result critically found that the chordwise positioning, vane height and array configuration were of prime importance. In contrast, the inclination angle, array packing density and vane shape in secondary importance.

Apart from the applications of the VGs, flaps have been also utilized to enhance the aerodynamic performance of wind turbines in recent years [49]. In addition to improving aerodynamic performance, they were preferred in the wind turbine community for load control. Stuart et al. [50] performed a numerical analysis of flap efficiency in reducing blade load at wind turbines, highlighting, in particular, their capability for load control and power augmentation. The NREL 5-MW turbine's dynamic load alleviation of flaps was the subject of intensive numerical analysis by Ng et al. [51], which effectively showed equivalent reductions in the blade-root bending moment and tip deflection of 12 and 20%. Furthermore, load alleviation was enhanced with sinusoidal flap deflection [52] and novel flap control strategies [53-56].

To date, employing VGs and flaps on wind turbine blades has admitted considerable attention, but independently. In addition to this attention, additional drag formation is inevitable in the independent usage of these mechanisms. Moreover, the combined impacts of VGs and flaps on the aerodynamic characteristics of wind turbine blades were unclear, rare, and even absent in the wind turbine literature. In this context, this study will be the first time to the combined impacts of the VGs and the flaps on the aerodynamic performance of wind turbine blades. Consequently, the objective of this study is to ensure a deep understanding of when those two passive flow control techniques are employed on wind turbine blades at the same time. Numerical simulations which were validated with experimental data were performed to identify flow characteristics formed on the surface of the uncontrolled S809 airfoil (without VG and flap). In what follows, the integrated mechanism of the VG and the flap over the S809 airfoil was investigated by simulating at Reynolds numbers of 0.4×10^5 and 1.2×10^5. In this system, the flap motion triggered the VG and activated the VG when needed at low speeds. Thus, this flap mechanism eliminated the unnecessary drag force generation when the VGs were not needed. In the simulations, the S809 airfoil with VGs (model-1), S809 airfoil with trailing-edge flap (model-2) and S809 airfoil with the integrated case (model-3) were considered.

Concerning the essential path of this study, a literature study was conducted to figure out the airfoil type and to see which type of studies about passive flow control with VGs and flaps in advance. This was shown in Section 1 of the paper. Section 2 consisted of the material and methods including test airfoil, and numerical simulation. The obtained data from the numerical simulation were post-processed, evaluated and then discussed in Section 4. The final remarks were provided in the conclusion section.

2. Material and methods

2.1. Airfoil model

In this study, the most well-known NREL S809 airfoil which is the most preferred in the wind turbine community is selected [43]. As mentioned earlier, the objective of this study was to examine aerodynamic performance as well as flow structure formed on S809 with integrated passive flow controllers such as VGs and trailing-edge flaps compared to the baseline model. In this context, as illustrated in Fig. 1, the baseline S809 airfoil and its controlled configurations like VGs, trailing-edge flap and integrated cases were investigated, respectively. In terms of better understanding how the integrated S809 airfoil worked, the figures were illustrated in 3D, whilst all numerical simulations were performed in 2D. For all cases, the chord (c) and span (s) lengths were 200 mm and 200 mm, respectively. In this study, the controlled S809 airfoil was compared to the baseline model at Reynolds numbers of 0.4×10^5 and 1.2×10^5. As technical information of the S809 airfoil with VGs in Fig. 1(b), the VGs were mounted along a straight line at 25% chord-wise close to the leading edge of the airfoil, the height of VGs was determined as 0.5 mm and the length was determined as 4 mm [57]. As the geometrical parameter of the S809 airfoil with trailing-edge flap in Fig. 1(c), it was obtained by cutting from the point 30% chord-wise close to the trailing edge of the airfoil. The VGs of the integrated airfoil were of the same size as those shown in figure b, and their flap dimensions were identical to those shown in figure c. Hereinafter, S809 with VGs, S809 with trailing-edge flap and S809 with the integrated case were referred to as model-1, model-2 and model-3, respectively.

2.2. Numerical analysis

Related to the numerical model, the Reynolds-averaged Navier Stokes (RANS) with the laminar kinetic energy model was utilized to analyze the low Reynolds number flow in this study [58]. The newly developed *k-kl-ω* model is a three-equation eddy-viscosity type, which contains transport equations for turbulent kinetic energy (k_T), laminar kinetic energy (k_L), and the inverse turbulent time scale (ω). The equations were solved by ANSYS-Fluent 18.2 solver. This model was selected because it was found to be too reasonable in terms of better estimation of the formation of laminar separation bubble (LSB), flow separation and reattachment as well as transition to turbulence [59,60]. Concerning the domain and mesh generation as denoted in Fig. 2, the flow domain as well as mesh distribution near the airfoil and its surfaces were ensured. The domain dimensions were obtained in pursuance of the airfoil's diameter, as was performed in our previous studies [61–63]. The airfoil was positioned 10 c from the inlet and 20 c from the outlet. It was pointed out that the length of the wake region of the airfoil was larger to provide a full development of the wake in the downstream

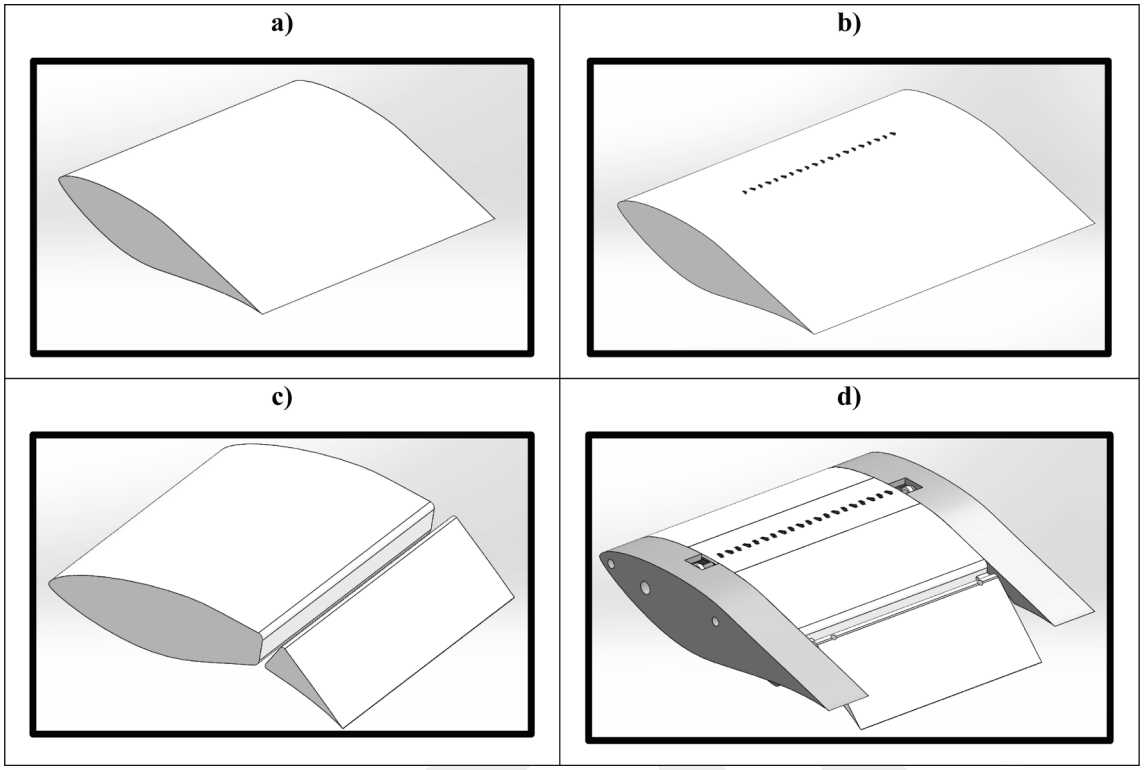

Fig. 1. Types of investigated airfoils, a) Baseline (the uncontrolled case), b) S809 with VGs, c) S809 with trailing-edge flap, d) S809 with integrated case (VGs + trailing-edge flap).

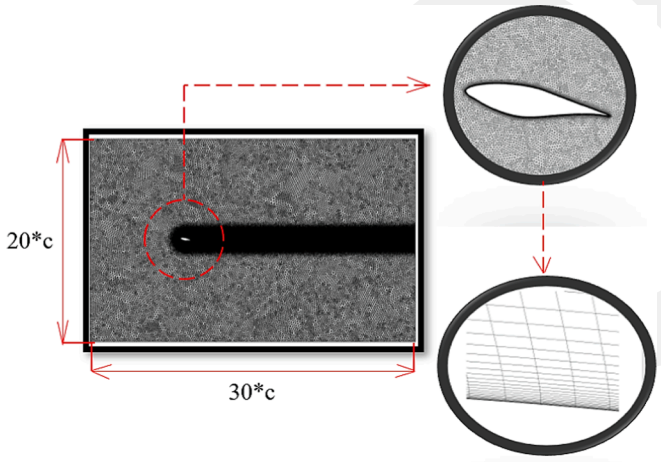

Fig. 2. The schematic of the flow domain with its close views.

region. The inlet and outlet were 20 c wide; the walls were 30 c wide. U_∞ = 3.58, 10.74 m/s was at the inlet, constant pressure was at the outlet, and stationary non-slip conditions were on the turbine and flow domain walls. The first layer thickness of the mesh structure was 1×10^{-4} mm and inflation layers at a growth rate of 1.2 were applied. The maximum y+ value around the airfoil was about 2 which was suitable for reasonable results. The y+ values over the airfoil were between 0.05 and 1 except for the leading edge. In addition, a tetra mesh structure was utilized. The selected convergence criterion for the residuals was 1.0×10^{-6}. The second-order upwind approach was employed to produce spatial discretization and provide minimum numerical diffusion after selecting the Semi-Implicit Method for Pressure Linked Equations-Consistent (SIMPLEC) solution methodology. The physical properties of flow inside the domain were mainly its dynamic viscosity and density taken as $\mu = 1.79 \times 10^{-5}$ kg/m.s and $\rho = 1$ kg/m^3 respectively. Detailed information concerning computational mesh was ensured as seen in Table 1.

Related to the mesh independency and validation studies as indicated in Fig. 3, the drag coefficient was taken into consideration for a proper number of elements. It was seen that the drag coefficient was nearly 0.085 when the number of elements was 0.1×10^6. In what follows, the drag coefficient decreased gradually when the number of elements increased until 1×10^6. After 1×10^6, the drag coefficient was approximately constant, and its value was 0.048. Furthermore, this value was well matched with the experimental findings performed by Qu et al. [64]. Hence, 1×10^6 was accepted as the number of elements in this study. Additionally, the numerical simulation for mesh independency was conducted at Reynolds number of 1.1×10^5, $\alpha = 10^\circ$ so as to compare same values of parameters from the study of Qu et al. [64].

3. Results and discussions

3.1. Aerodynamic performance results

This section presented the aerodynamic performance of the

Table 1
Main properties of the computational mesh.

Airfoil	NREL S809
Chord length c	0.2 m
VG height h	0.5 mm
VG position	0.25*c
Flap position	0.7*c
Flow velocity	3.58 and 10.74
Reynolds number	0.4×10^5 and 1.2×10^5
First layer spacing	1×10^{-4}
y^+	1
Far-field distance	30*c
Normal growth ratio	1.2

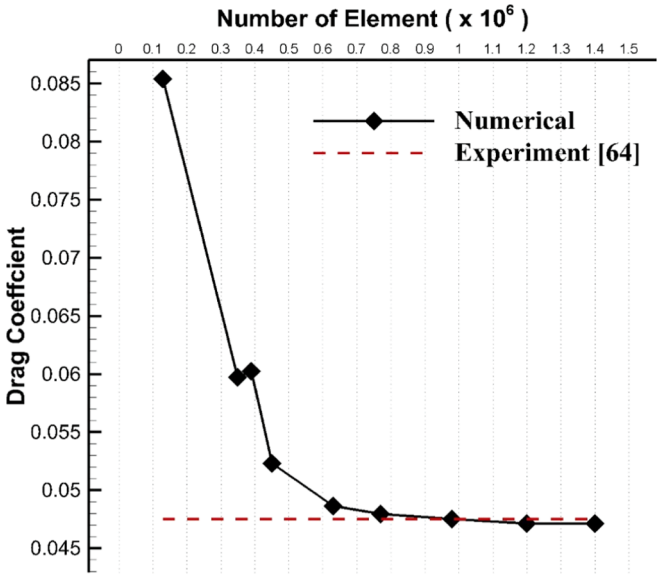

Fig. 3. Mesh independence, Re = 1.1 × 10^5, α = 10°.

controlled S809 airfoil compared to the baseline model at Reynolds numbers of 0.4 × 10^5 and 1.2 × 10^5. The comparison of different settings in terms of aerodynamic performance effects was shown in Fig. 4(a). The results demonstrated that C_L values belonging to model-2 and model-3 were higher than baseline and model-1. At Re = 0.4 × 10^5, utilizing only VGs on the surface of the airfoil did not influence so much in terms of aerodynamic performance compared to the baseline. On the other hand, the aerodynamic performance of employing only flap with β = 30° was higher than model-3 when α < 8°. When α > 8°, both employing VGs and flap on airfoil boosted aerodynamic performance enormously. In particular, aerodynamic performance enhanced by ~ 18% and 20% at α = 10° and α = 12°, respectively. When Re = 1.2 × 10^5 as seen in Fig. 4 (b), model-2 exhibited the highest aerodynamic performance compared to the other configurations and baseline model. In addition to the lift coefficient enhancement, the drag coefficients of the baseline model and model-1 were less than other configurations for both Reynolds numbers as demonstrated in Fig. 5 due to the flow control. Additionally, it was observed that the drag coefficient of model-2 varied much more than other configurations with changing angles of attack. This most probably showed that flap motion at model-2 exhibited a more dominant role variation of velocity and pressure amounts on the surface of the airfoil. In contrast to model-2, the curve of drag coefficient belonging to model-1 did not change with varying angles of attack and even it kept its trends with the curve of drag coefficient trend belonging to the baseline model.

3.2. *Discussion of u/U_∞ and streamlines belonging to model-3 configuration*

In this study, the logic of the integrated system was as follows: the flap and the VG were in the open position when the wind turbine was not operating, and the flap was closed up due to the moment of inertia of the flow with the increase of wind speed. The VG connected to the flap with a mechanism also entered its slot in the blade thanks to the flap closing. Thus, at low wind speeds, the flap and the VG provided an improvement in low Reynolds number flow around the turbine blade, and the flap angle and the VG height decreased as the wind velocity increased. These reductions decreased unnecessary drag formation. When the wind speed had enough inertia to bring the flap to the fully closed position, both the flap and the VG were hidden and drag formation was prevented. When the wind speed decreased again, the integrated system with a spring mechanism came into operation again and supplied control of the flow.

To explain the flow phenomena, in Fig. 6 and Fig. 7, the values of C_L/C_D with varying of β for the model-3 were demonstrated at different Reynolds numbers and α = 4°. Furthermore, C_L/C_D graphs were supported with the velocity contours corresponding to different β angles. When Re was 0.4 × 10^5, it was observed that C_L/C_D gradually decreased as the flap angle decreased from β = 30° to β = 0°. Especially, the simultaneous motion of VGs and the flap at model-3 caused greater C_L/C_D to form at higher flap angles. However, it was seen that C_L/C_D was nearly 2.1 when β = 0°, resulting in the presence of the lowest aerodynamic performance at this flap angle. When Re = 1.2 × 10^5, the opposite curve trend according to the previous situation occurred at Re = 0.4 × 10^5 appeared. At β = 30° to β = 20°, the values of C_L/C_D were 5.7 and 5.8, respectively. Afterwards, the C_L/C_D curve displayed a gradual upward shift by utilizing both the VGs and the trailing-edge flap. As physically explained, it could be inferred that working both the VGs and trailing-edge flap together at a lower Reynolds number caused the pressure in the lower surface to be high when the flap angle was higher (inherently maximum VGs height), resulting in presence of maximum

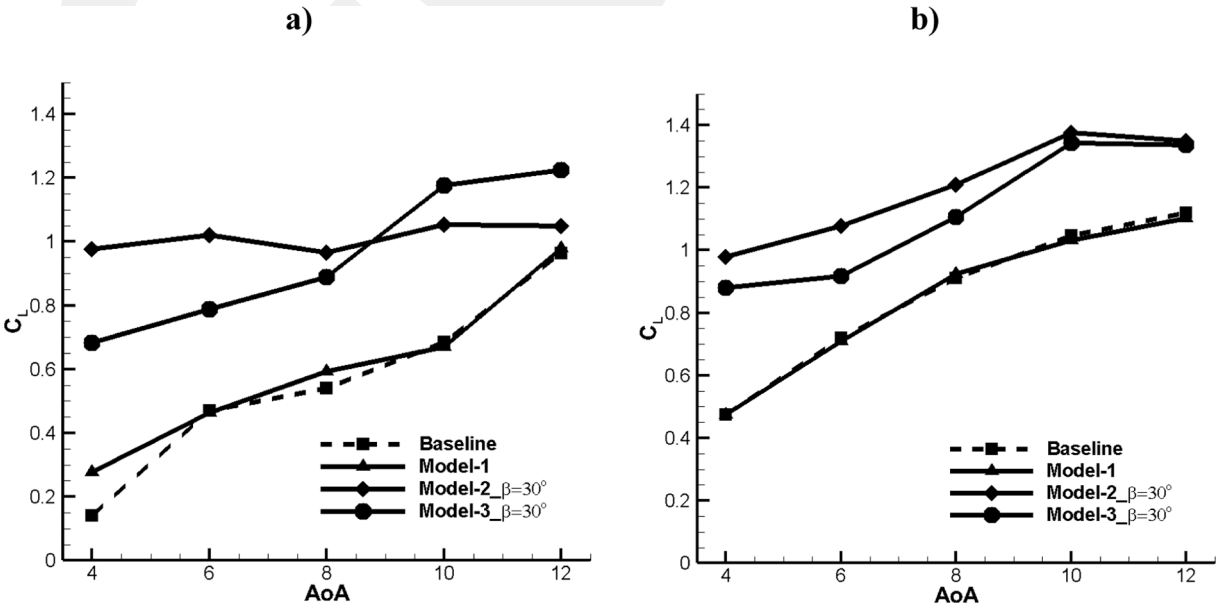

Fig. 4. Lift (C_L) coefficient graphs, a) Re = 0.4 × 10^5, b) 1.2 × 10^5.

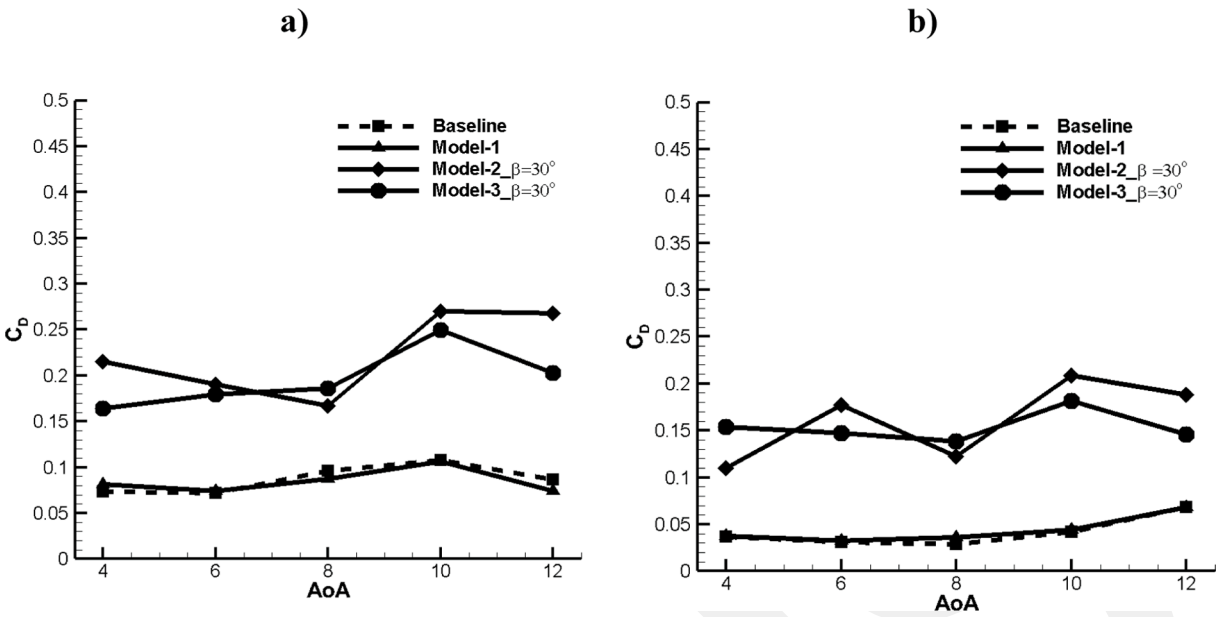

Fig. 5. Drag (C_D) coefficient graphs, a) Re = 0.4×10^5, b) 1.2×10^5.

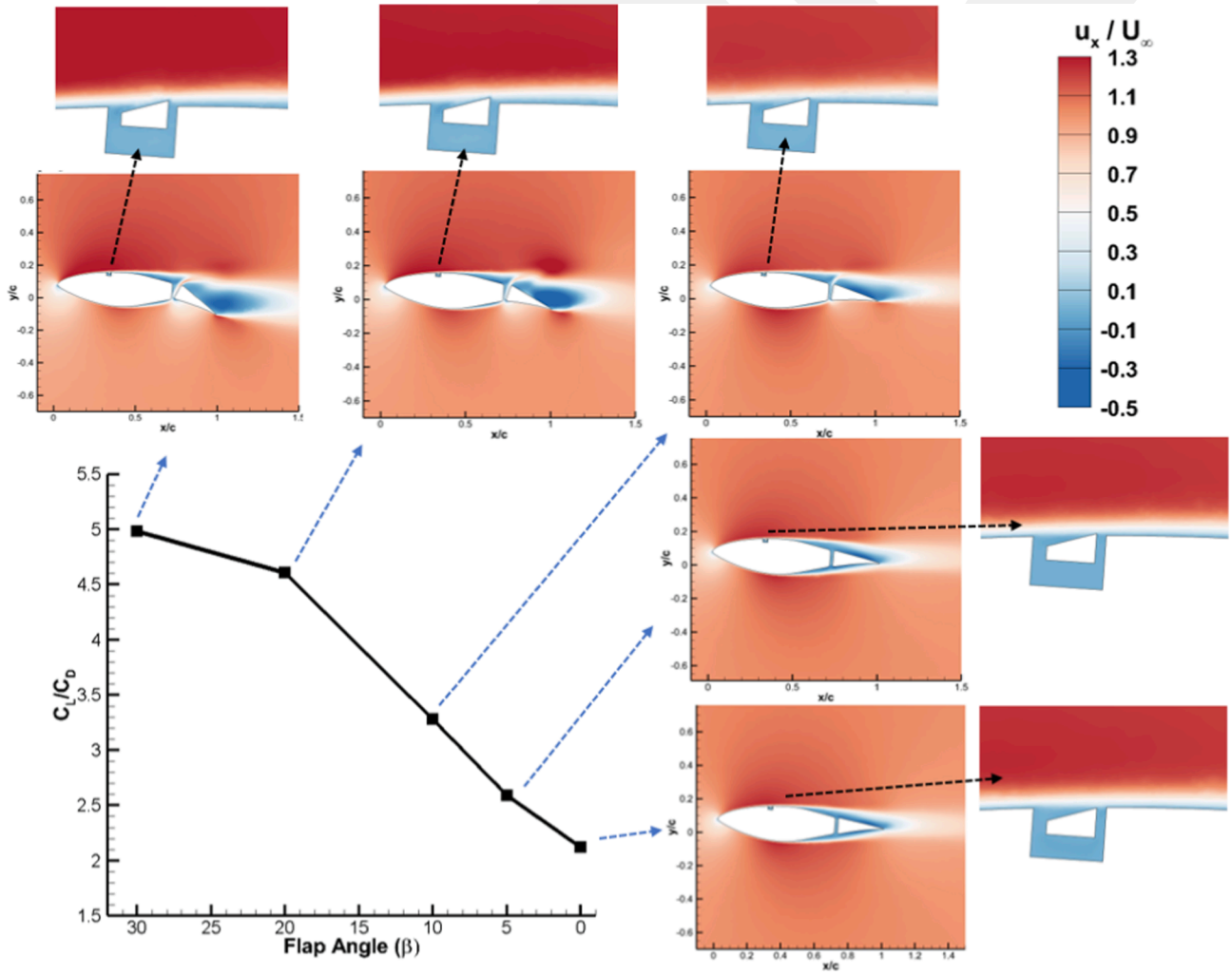

Fig. 6. The results at different positions of flap and VGs integrated system (model-3), at Re = 0.4×10^5, α = 4°.

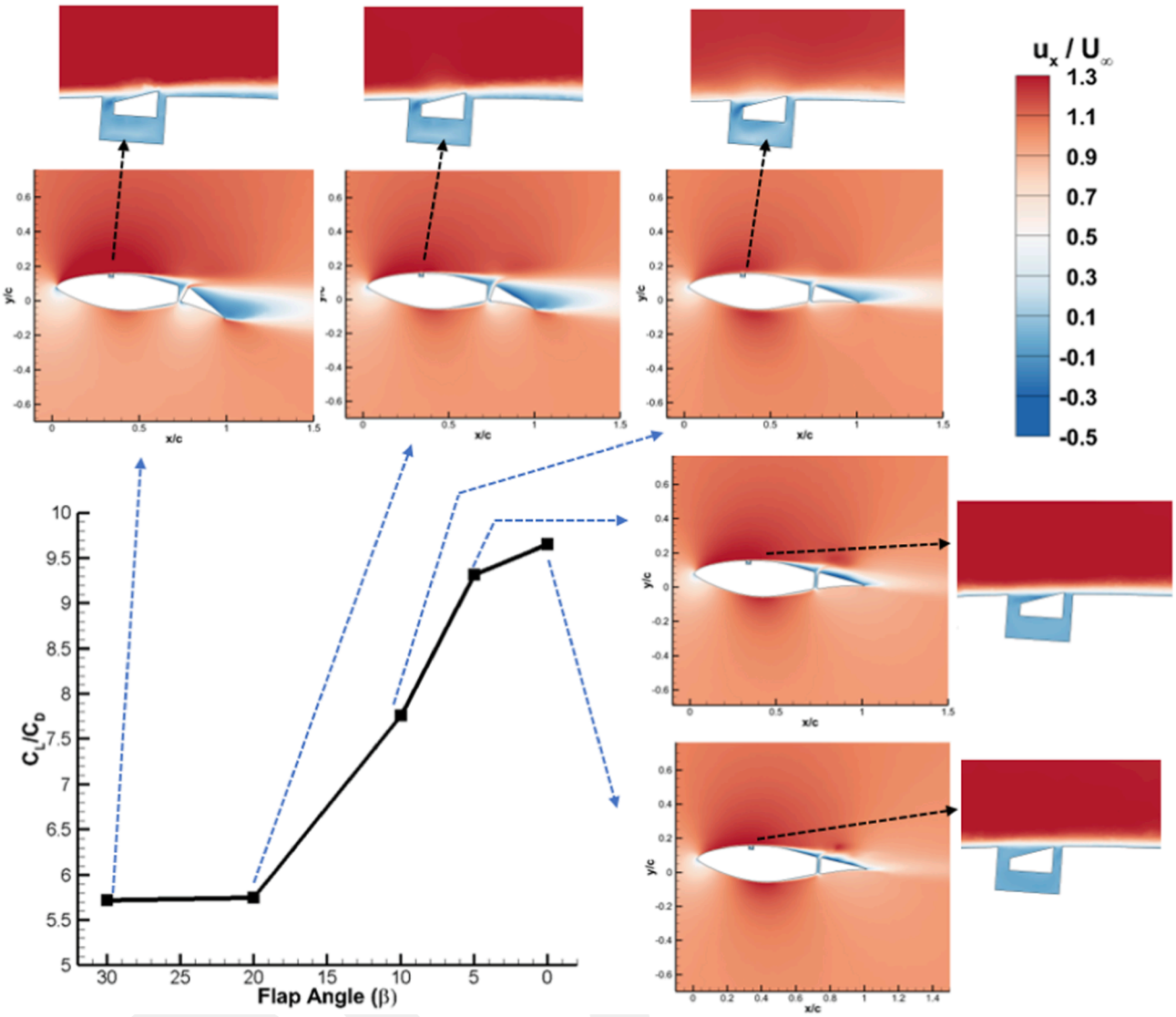

Fig. 7. The results at different positions of flap and VGs integrated system (model-3), at Re = 1.2 × 10^5, α = 4°.

pressure difference among the airfoil surfaces. Moreover, hiding the VGs-trailing edge combination provided the drag reduction and therefore C_L/C_D increased at smaller flap angles when the Reynolds number was relatively higher.

2D streamlines as well as vortices in the wake region of model-3 configuration were investigated to explain the results as illustrated in Fig. 8. The results were provided according to different Reynolds numbers and trailing-edge flap angles. When Re = 0.4 × 10^5 and β = 0°, adverse pressure gradients had a dominant impact on boundary layer and it was observed that there was boundary layer flow separation at the middle part of the airfoil because of existing of those negative effects of adverse pressure gradients. Furthermore, flow vortices existed at both sides of the trailing-edge flap. The flow vortices on the flap caused the vortex shedding to form. Those flow vortices moved towards the wake region of the airfoil, resulting in an existing larger wake size at a lower Reynolds number. However, this larger wake size turned into a narrower wake region where the influence of vortex shedding reduced when Reynolds number (flow velocities) increased. As expected, the size of flow circulation on the surface of the trailing-edge flap was bigger with increasing the flap angle to β = 30°. If the flap angle is increased further, flow separations on both the flap and the wing increase and the stall on the blade may occur. Similar behavior was also observed for Re = 1.2 × 10^5. However, the size of flow circulation was relatively smaller than those that occurred at Re = 0.4 × 10^5 since increasing the Reynolds number (flow velocity) caused inertial forces to be more dominant than viscous forces.

In terms of better understanding, the flow characteristics formed on Model-3 configuration, turbulence statistics including distributions of laminar kinetic energy and turbulence intensity were comprehensively considered at different Reynolds numbers and trailing-edge flap angles as depicted in Fig. 9 and Fig. 10, respectively. As seen in these figures, when the flap and VG operated at β = 30°, the laminar and turbulent kinetic energies increased, and both the flap and VG triggered the vortex formations. Those laminar and turbulent kinetic energies identify the number of fluctuations because of the presence of small and larger eddies in the boundary layer [59,61,65]. Besides, the flow over the airfoil was the attached flow as the Reynolds number was raised.

3.3. Evaluation of power efficiency of the model-3 configuration

Improvement in the aerodynamic performance of the blade points out to an increase in the energy output of wind turbines. In terms of energy conversion, the power efficiency (PE) of the model-3 was calculated by using Equation (1) [20,66]:

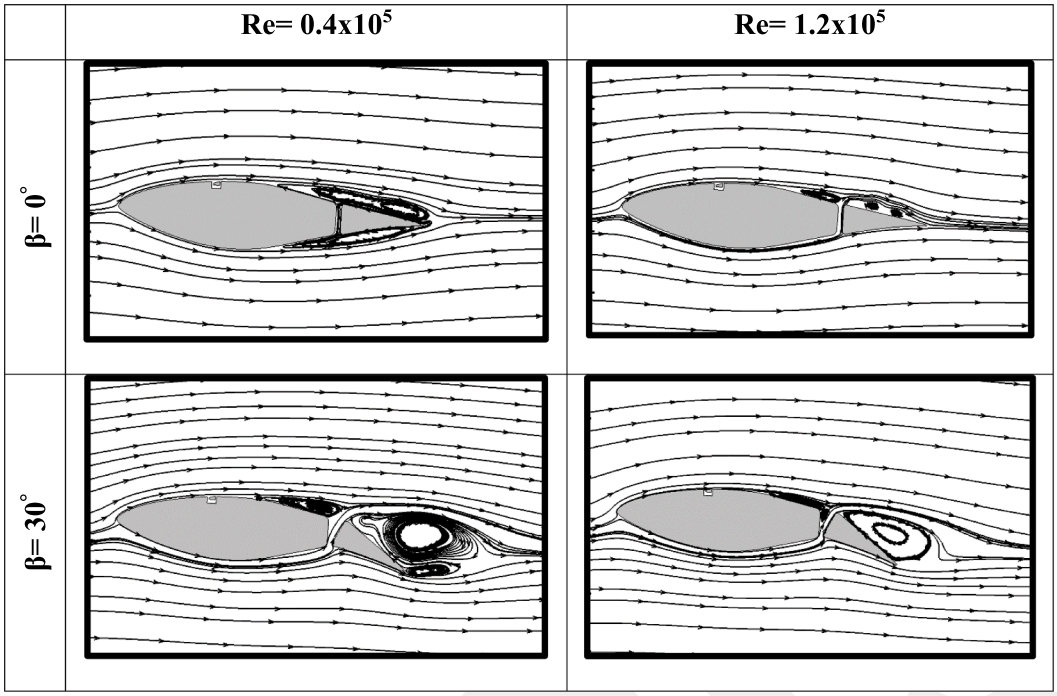

Fig. 8. Streamlines of model-3 configuration at different Reynolds numbers and flap angles.

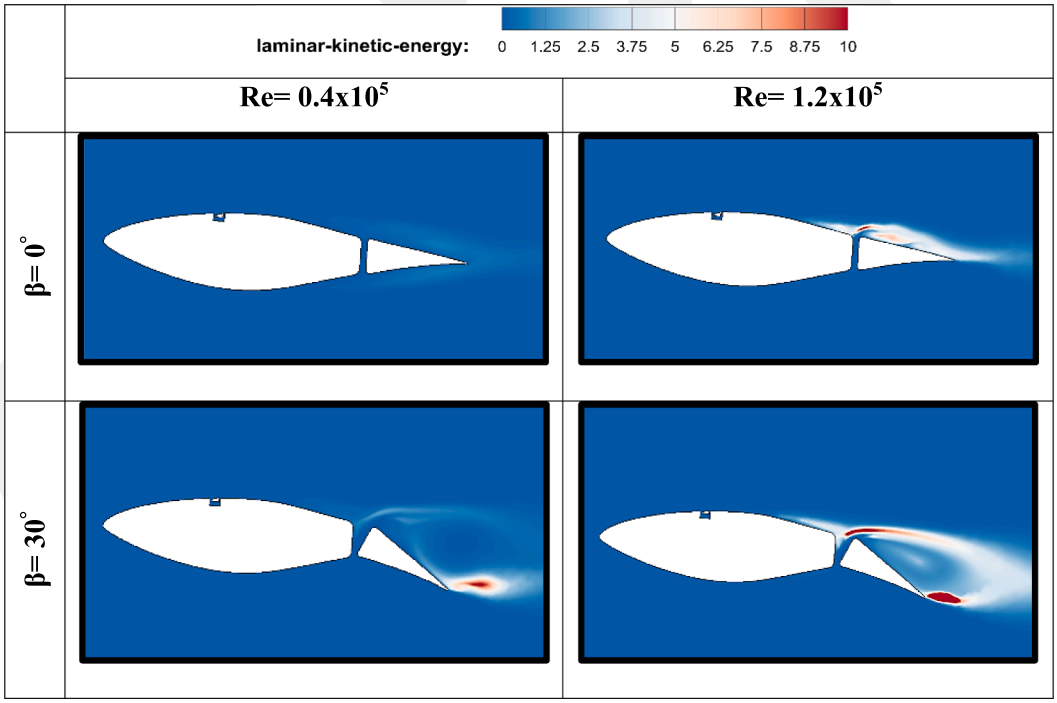

Fig. 9. Contour plots of laminar kinetic energy at different Reynolds numbers and flap angles.

$$\mathrm{PE} = \frac{C_L^{3/2}}{C_D} \tag{1}$$

To compare the power efficiency at low speed with that at high speed for $\alpha = 4°$, Fig. 11 was given. When the flap and VGs were off ($\beta = 0°$), the calculated power efficiency from aerodynamic force coefficients was 3.18 at low wind speed. By utilizing the flap-VG integrated mechanism, the power efficiency was raised to 7.48 with an increment of 135%. As in the classical practice of wind turbines if the VGs fixed on the wind turbine blade, the power efficiency was 8.58 at high wind speed, while this value was raised to 14.47 with an increment of 69% if the flap and the VGs were closed by using the integrated mechanism. As mentioned before, this mechanism will be placed inside the blade with a spring mechanism and the wind turbine will operate while the flap and VGs are open at low speeds, and the power efficiency raised owing to the flap and VGs at low speeds. Then, with the increase in wind speed, the flaps and VGs will close automatically (without additional energy demand) thanks to wind inertia, and unnecessary aerodynamic performance reduction will be prevented. If the wind speed decrease again, the spring

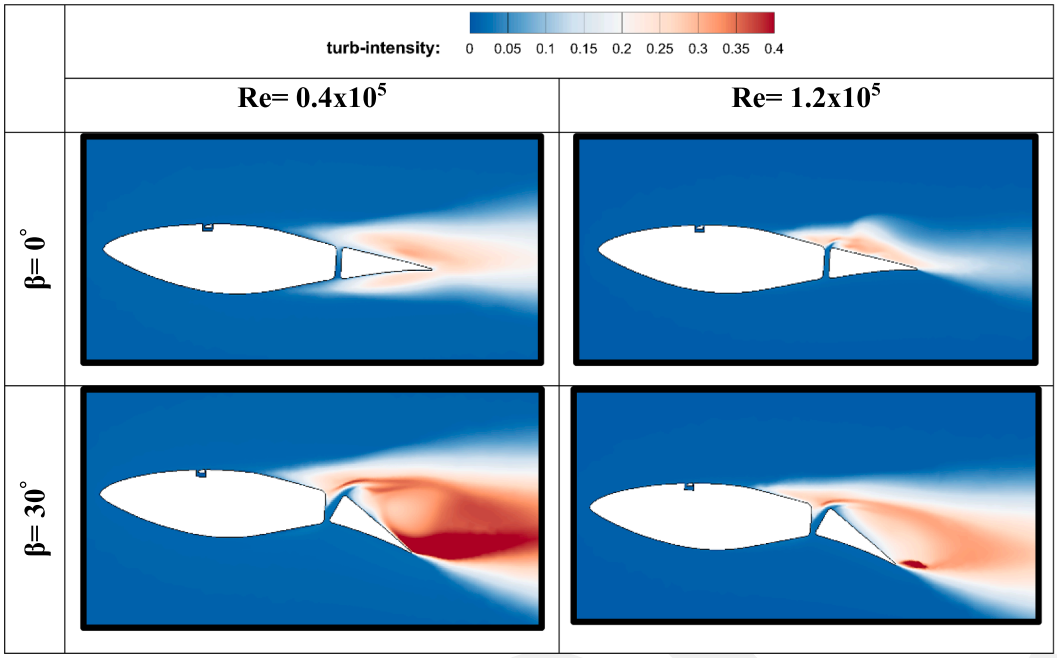

Fig. 10. Contour plots of turbulent intensity at different Reynolds numbers and flap angles.

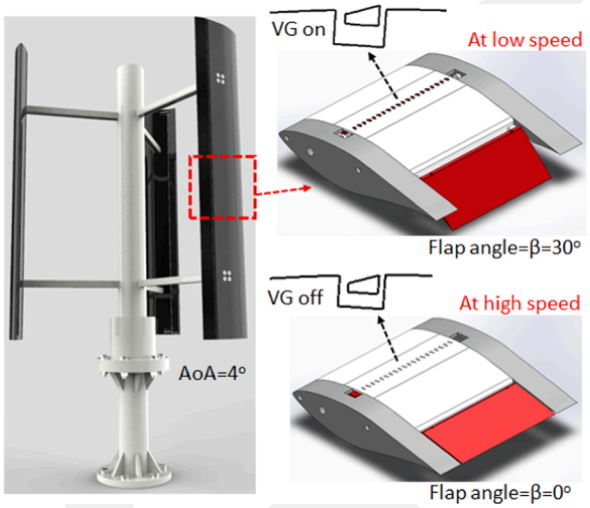

Wind Speed	Power Efficiency $(C_L^{3/2}/C_D)$		Rate of Increase
V= 3.58 m/s (Re: 0.4 x10^5)	**7.48**	**3.18**	**135%**
V= 10.74 m/s (Re: 1.2 x10^5)	**8.58**	**14.47**	**69%**
Flap Angle	β=30°	β=0°	

Fig. 11. Power efficiency improvement of the model-3 at different Reynolds numbers and flap angles.

mechanism will bring the flap and Vg back to the open position. Therefore, with this patent-protected idea [67], the power efficiency in the wind turbine will be used to the maximum in any case, as can be seen in Fig. 11.

4. Conclusion

In this study, the integrated flap-VG mechanism was considered to control the low Reynolds number viscous flow over the wind turbine blade airfoil. The VG was connected to the flap with a mechanism assumed to enter its slot in the blade based on the flap closing. Thereby, the flap and the VG planned to provide an improvement at low wind speeds, then the flap angle and the VG height decreased as the wind speed increased to prevent to unnecessary drag formation. The result pointed out that the lift drag ratio of the S809 airfoil without a flow controller (baseline case) was $C_L/C_D = 1.9$ at a Reynolds number of 0.4×10^5. The lift drag ratio at the same Reynolds number was found as $C_L/C_D = 3.4$, $C_L/C_D = 4.5$ and $C_L/C_D = 4.16$ for S809 airfoil with model-1, model-2 and model-3, respectively. At Reynolds number of 1.2×10^5, C_L/C_D of baseline case was 12.8. This ratio was determined as 12.7, 8.9, and 5.71 for S809 airfoil with model-1, model-2 and model-3, respectively. It resulted that working both the VGs and trailing-edge flap together (model-3) at a lower Reynolds number caused the pressure gradient on the pressure surface to be high when the flap angle was higher (inherently maximum VGs height), resulting in presence of maximum pressure difference among the airfoil surfaces. Moreover, hiding the VGs-trailing edge combination provided the drag reduction and therefore C_L/C_D increased at smaller flap angles when Reynolds number was relatively higher.

In terms of energy output improvement, it was shown that this novel idea provided more energy output in this study. When the flap and VGs were off, the power efficiency was 3.18 at low wind speed. By utilizing the flap-VG integrated mechanism, the power efficiency was raised to 7.48. As in the classical practice of wind turbines if the VGs fixed on the wind turbine blade, the power efficiency was 8.58 at high wind speed, while this value was raised to 14.47 if the flap and the VGs were closed

by using the integrated mechanism. With this mechanism placed inside the blade with a spring mechanism, the flap and VGs will be open position at low speeds. Then, with the increase in wind speed, the flaps and VGs will close automatically. If the wind speed decrease again, the spring mechanism will bring the flap and Vg back to the open position. Therefore, with this patent-protected idea, the power efficiency in the wind turbine will be able to use to the maximum at every wind speed.

CRediT authorship contribution statement

Mustafa Özden: Methodology, Investigation, Validation, Conceptualization, Data curation, Formal analysis, Visualization, Writing - original draft. **Mustafa Serdar Genç:** Project administration, Conceptualization, Methodology, Investigation, Supervision, Data curation, Formal analysis, Funding acquisition, Validation, Visualization, Writing - review & editing. **Kemal Koca:** Investigation, Data curation, Writing - original draft.

Declaration of Competing Interest

The authors declare that they have no known competing financial interests or personal relationships that could have appeared to influence the work reported in this paper.

Data availability

No data was used for the research described in the article.

Acknowledgement

The authors thank the Scientific and Technological Research Council of Turkey (TÜBİTAK) for the Doctoral Scholarship for Priority Areas 2211-C for Dr. Mustafa ÖZDEN.

References

[1] Zhang H, Wen J, Zhan J, Xin D. Effects of blade number on the aerodynamic performance and wake characteristics of a small horizontal-axis wind turbine. Energ Conver Manage 2022;273:116410.
[2] Su R, Gao Z, Chen Y, Zhang C, Wang J. Large-eddy simulation of the influence of hairpin vortex on pressure coefficient of an operating horizontal axis wind turbine. Energ Conver Manage 2022;267:115864.
[3] Özkan R, Genç MS. Aerodynamic design and optimization of a small-scale wind turbine blade using a novel artificial bee colony algorithm based on blade element momentum (ABC-BEM) theory. Energ Conver Manage 2023;283:116937.
[4] Genç MS, Koca K, Açıkel HH, Özkan G, Kırış MS, Yıldız R. Flow characteristics over NACA4412 airfoil at low Reynolds number. EPJ web of conferences 2016;114:02029.
[5] Miao W, Liu Q, Xu Z, Yue M, Li C, Zhang W. A comprehensive analysis of blade tip for vertical axis wind turbine: Aerodynamics and the tip loss effect. Energ Conver Manage 2022;253:115140.
[6] Barlas TK, van Kuik GA. Review of state of the art in smart rotor control research for wind turbines. Prog Aerosp Sci 2010;46(1):1–27.
[7] Liu Q, Miao W, Bashir M, Xu Z, Yu N, Luo S, et al. Aerodynamic and aeroacoustic performance assessment of a vertical axis wind turbine by synergistic effect of blowing and suction. Energ Conver Manage 2022;271:116289.
[8] Genç MS, Açıkel HH, Akpolat MT, Özkan G, Karasu İ. Acoustic control of flow over NACA 2415 aerofoil at low Reynolds numbers. Journal of Aerospace Engineering-ASCE 2016;29(6):04016045.
[9] Genç MS, Açıkel HH. Flow control with perpendicular acoustic forcing on NACA 2415 aerofoil at low Reynolds numbers. Proc IMechE, Part G- J Aerospace Eng 2016;230:2447–62.
[10] Ge M, Zhang H, Wu Y, Li Y. Effects of leading-edge defects on aerodynamic performance of the S809 airfoil. Energ Conver Manage 2019;195:466–79.
[11] Genç MS, Koca K, Demir H, Açıkel HH. Traditional and new types of passive flow control techniques to pave the way for high maneuverability and low structural weight for UAVs and MAVs. Autonomous Vehicles 2020:131–60.
[12] Roy S, Das B, Biswas A. Effect of leading-edge protrusion shapes for passive flow control measure on wind turbine blades. Ocean Eng 2023;269:113688.
[13] Genç MS, Koca K, Acikel HH. Investigation of pre-stall flow control on wind turbine blade airfoil using roughness element. Energy 2019;176:320–34.
[14] Miao X, Zhang Q, Wang L, Jiang H, Qi H. Application of riblets on turbine blade endwall secondary flow control. J Propul Power 2015;31(6):1578–85.
[15] Wang H, Mao X, Liu B, Qing Y. Combined flow control with full-span slot and end-wall boundary layer suction in a large-camber compressor cascade. Aerosp Sci Technol 2021;119:107121.
[16] Sedighi H, Akbarzadeh P, Salavatipour A. Aerodynamic performance enhancement of horizontal axis wind turbines by dimples on blades: Numerical investigation. Energy 2020;195:117056.
[17] Frohnapfel B, Jovanović J, Delgado A. Experimental investigations of turbulent drag reduction by surface-embedded grooves. J Fluid Mech 2007;590:107–16.
[18] Demir M, Genç MS. An experimental investigation of laminar separation bubble formation on flexible membrane wing. Eur J Mech B/Fluids 2017;65:326–38.
[19] Açıkel HH, Genç MS. Control of Laminar Separation Bubble over Wind Turbine Airfoil Using Partial Flexibility on Suction Surface. Energy 2018;165:176–90.
[20] Açıkel HH, Genç MS, Koca K. Effect of partial flexibility over both upper and lower surfaces to flow over wind turbine airfoil. Energ Conver Manage 2020;219:113042.
[21] Koca K, Genç MS, Bayır E, Soğuksu FK. Experimental study of the wind turbine airfoil with the local flexibility at different locations for more energy output. Energy 2022;239:121887.
[22] Koca K, Genç MS, Ertürk S. Impact of local flexible membrane on power efficiency stability at wind turbine blade. Renew Energy 2022;197:1163–73.
[23] Koca K, Genç MS, Veerasamy D, Özden M. Experimental flow control investigation over suction surface of turbine blade with local surface passive oscillation. Ocean Eng 2022;266:113024.
[24] Bodling A, Sharma A. Numerical investigation of noise reduction mechanisms in a bio-inspired airfoil. J Sound Vib 2019;453:314–27.
[25] Hansen KL, Kelso RM, Dally BB. Performance variations of leading-edge tubercles for distinct airfoil profiles. AIAA J 2011;49(1):185–94.
[26] Wang J, Nakata T, Liu H. Development of mixed flow fans with bio-inspired grooves. Biomimetics 2019;4(4):72.
[27] Rostamzadeh N, Kelso RM, Dally BB, Hansen KL. The effect of undulating leading-edge modifications on NACA 0021 airfoil characteristics. Phys Fluids 2013;25(11):117101.
[28] Joseph J, Sathyabhama A. Leading edge tubercle on wind turbine blade to mitigate problems of stall, hysteresis, and laminar separation bubble. Energ Conver Manage 2022;255:115337.
[29] Huang S, Qiu H, Wang Y. Aerodynamic performance of horizontal axis wind turbine with application of dolphin head-shape and lever movement of skeleton bionic airfoils. Energ Conver Manage 2022;267:115803.
[30] Wang Z, Wang Y, Zhuang M. Improvement of the aerodynamic performance of vertical axis wind turbines with leading-edge serrations and helical blades using CFD and Taguchi method. Energ Conver Manage 2018;177:107–21.
[31] Jiang R, Zhao Z, Liu Y, Liu H, Ma Y, Wang T, et al. Effect of vortex generator orientation on wind turbines considering the three-dimensional rotational effect. Ocean Eng 2023;267:113307.
[32] Cheawchan A, Mohamed MA, Ng BF, New TH. Flow Structures of Wishbone Vortex Generators and Their Interactions with a Backward-Facing Ramp. J Aerosp Eng 2023;36(1):04022120.
[33] Zhao Z, Jiang R, Feng J, Liu H, Wang T, Shen W, et al. Researches on vortex generators applied to wind turbines: A review. Ocean Eng 2022;253:111266.
[34] Heragy M, Kono T, Kiwata T. Investigating the effects of wind concentrator on power performance improvement of crossflow wind turbine. Energ Conver Manage 2022;255:115326.
[35] Jiang Y, Zhao P, Stoesser T, Wang K, Zou L. Experimental and numerical investigation of twin vertical axis wind turbines with a deflector. Energ Conver Manage 2020;209:112588.
[36] Zhao P, Jiang Y, Liu S, Stoesser T, Zou L, Wang K. Investigation of fundamental mechanism leading to the performance improvement of vertical axis wind turbines by deflector. Energ Conver Manage 2021;247:114680.
[37] Saleem A, Kim M. Effect of rotor tip clearance on the aerodynamic performance of an aerofoil-based ducted wind turbine. Energ Conver Manage 2019;201:112186.
[38] Hosseini A, Goudarzi N. Design and CFD study of a hybrid vertical-axis wind turbine by employing a combined Bach-type and H-Darrieus rotor systems. Energ Conver Manage 2019;189:49–59.
[39] Gao L, Zhang H, Liu Y, Han S. Effects of vortex generators on a blunt trailing-edge airfoil for wind turbines. Renew Energy 2015;76:303–11.
[40] Manolesos M, Voutsinas SG. Experimental investigation of the flow past passive vortex generators on an airfoil experiencing three-dimensional separation. J Wind Eng Ind Aerodyn 2015;142:130–48.
[41] Taylor HD. The elimination of diffuser separation by vortex generators. United Aircraft Corporation; 1947. Technical Report No. 4012-3.
[42] Nickerson, JR, J. A study of vortex generators at low Reynolds numbers. In: 24th Aerospace Sciences Meeting; 1986, pp. 155.
[43] Timmer WA, Van Rooij RPJOM. Summary of the Delft University wind turbine dedicated airfoils. J Sol Energy Eng 2003;125(4):488–96.
[44] Wang H, Zhang B, Qiu Q, Xu X. Flow control on the NREL S809 wind turbine airfoil using vortex generators. Energy 2017;118:1210–21.
[45] Zhu C, Qiu Y, Feng Y, Wang T, Li H. Combined effect of passive vortex generators and leading-edge roughness on dynamic stall of the wind turbine airfoil. Energ Conver Manage 2022;251:115015.
[46] Lin JC. Review of research on low-profile vortex generators to control boundary-layer separation. Prog Aerosp Sci 2002;38(4–5):389–420.
[47] Fouatih OM, Medale M, Imine O, Imine B. Design optimization of the aerodynamic passive flow control on NACA 4415 airfoil using vortex generators. Eur J Mech-B/Fluids 2016;56:82–96.
[48] Baldacchino D, Ferreira C, Tavernier DD, Timmer WA, Van Bussel GJW. Experimental parameter study for passive vortex generators on a 30% thick airfoil. Wind Energy 2018;21(9):745–65.

[49] Berg DE, Zayas JR, Lobitz DW, van Dam CP, Chow R, Baker JP. Active aerodynamic load control of wind turbine blades. In Fluids Eng Division Summer Meeting 2007; 42894:1119–27.
[50] Stuart JG, Wright AD, Butterfield CP. Considerations for an integrated wind turbine controls capability at the national wind technology center: An aileron control case study for power regulation and load mitigation (No. NREL/TP-440-21335; CONF-960630-2). National Renewable Energy Lab. (NREL), Golden, CO (United States); 1996.
[51] Ng BF, Palacios R, Kerrigan EC, Graham JMR, Hesse H. Aerodynamic load control in horizontal axis wind turbines with combined aeroelastic tailoring and trailing-edge flaps. Wind Energy 2016;19(2):243–63.
[52] Oltmann NC, Sobotta D, Hoffmann A. Load reduction of wind turbines using trailing edge flaps. Energy Procedia 2017;136:176–81.
[53] Fischer A, Madsen HA. Investigation of the theoretical load alleviation potential using trailing edge flaps controlled by inflow data. Wind Energy 2016;19(9): 1567–83.
[54] Mansi A, Aydin D. The impact of trailing edge flap on the aerodynamic performance of small-scale horizontal axis wind turbine. Energ Conver Manage 2022;256:115396.
[55] Özden KS, Karasu İ, Genç MS. Experimental investigation of the ground effect on a wing without/with trailing edge flap. Fluid Dyn Res 2020;52(4):045504.
[56] Hao W, Bashir M, Li C, Sun C. Flow control for high-solidity vertical axis wind turbine based on adaptive flap. Energ Conver Manage 2021;249:114845.
[57] Bianchini A, Balduzzi F, Rosa DD, Ferrara G. On the use of Gurney Flaps for the aerodynamic performance augmentation of Darrieus wind turbines. Energ Conver Manage 2019;184:402–15.
[58] Özden M. Investigation of the effect of integrated flap-vortex generator mechanism on aerodynamic performance of the wind turbine blade. Erciyes University; 2022. PhD thesis.
[59] Walters DK, Cokljat D. A three-equation eddy-viscosity model for Reynolds-averaged Navier-Stokes simulations of transitional flow. J Fluids Eng 2008;130 (12).
[60] Choudhry A, Arjomandi M, Kelso R. A study of long separation bubble on thick airfoils and its consequent effects. Int J Heat Fluid Flow 2015;52:84–96.
[61] Karasu İ, Özden M, Genç MS. Performance assessment of transition models for three-dimensional flow over NACA4412 wings at low Reynolds numbers. J Fluids Eng 2018;140(12).
[62] Genç MS, Lock G, Kaynak Ü. An experimental and computational study of low Re number transitional flows over an aerofoil with leading edge slat, The 26th Congress of ICAS and 8th AIAA ATIO, AIAA-8877; 2008.
[63] Genç MS, Kaynak Ü. Control of laminar separation bubble over a NACA2415 aerofoil at low re transitional flow using blowing/suction. In: International Conference on Aerospace Sciences and Aviation Technology, ASAT-13, May 26–28, 2009.
[64] Qu H, Hu, J, Gao, X. The impact of Reynolds number on two-dimensional aerodynamic airfoil flow. In 2009 World Non-Grid-Connected Wind Power and Energy Conference; 2009. pp. 1-4.
[65] Genç MS, Kaynak Ü, Yapici H. Performance of transition model for predicting low Re aerofoil flows without/with single and simultaneous blowing and suction. Eur J Mech-B/Fluids 2011;30(2):218–35.
[66] Bleischwitz R, De Kat R, Ganapathisubramani B. Aspect-ratio effects on aeromechanics of membrane wings at moderate Reynolds numbers. AIAA Journal 2015;53(3):780–8.
[67] Genç MS, Özden M, Karasu İ, Sekhoune K. An Airfoil with Integrated Vortex Generator-Flap Self-Acting Based on Air Velocity, Turkish Patent and Trademark Office; 2017/23597.